



OPEN ACCESS

EDITED BY

Junjie Li,
Kyushu University, Japan

REVIEWED BY

Dan Shao,
South China University of Technology, China
Zhimin Chang,
Chinese Academy of Sciences (CAS), China

*CORRESPONDENCE

Tao Wang,
✉ echowong8921@126.com

RECEIVED 21 April 2025

ACCEPTED 29 May 2025

PUBLISHED 13 June 2025

CITATION

Feng C, Song S, Zhang X, Wang J, Meng Q and Wang T (2025) Ultrasound-controllable carbon monoxide nano-delivery systems for combined sonodynamic/gaseous therapies. *Front. Bioeng. Biotechnol.* 13:1615481. doi: 10.3389/fbioe.2025.1615481

COPYRIGHT

© 2025 Feng, Song, Zhang, Wang, Meng and Wang. This is an open-access article distributed under the terms of the [Creative Commons Attribution License \(CC BY\)](https://creativecommons.org/licenses/by/4.0/). The use, distribution or reproduction in other forums is permitted, provided the original author(s) and the copyright owner(s) are credited and that the original publication in this journal is cited, in accordance with accepted academic practice. No use, distribution or reproduction is permitted which does not comply with these terms.

Ultrasound-controllable carbon monoxide nano-delivery systems for combined sonodynamic/gaseous therapies

Chong Feng¹, Shuang Song¹, Xiaoyu Zhang², Jing Wang³, Qingxin Meng⁴ and Tao Wang^{4*}

¹Ultrasound Department of Hong Qi Hospital of Mudanjiang Medical University, Mudanjiang, China, ²Health Management Center, Mudanjiang First People's Hospital, Mudanjiang, China, ³Department of Biology, School of Basic Medical Sciences, Mudanjiang Medical University, Mudanjiang, China, ⁴Ultrasound Department of the Second Affiliated Hospital of Mudanjiang Medical University, Mudanjiang, China

Introduction: The integration of sonodynamic therapy (SDT) and carbon monoxide (CO) presents a promising synergistic strategy in cancer therapy owing to the unique advantage of CO in SDT sensitization. However, the development of SDT-compatible CO-delivery nanosystems remain a substantial challenge.

Methods: Here, we developed an ultrastable and controllable CO nanoreservoir system through the integration of chlorine e6 (Ce6)-loaded, cancer cell membrane coating and iron carbonyl ($\text{Fe}_3\text{CO}_{12}$)-bridged mesoporous silica bodies ($\text{Fe}_3\text{CO}_{12}$ -MSNs), which was specifically engineered to simultaneously achieve SDT and ultrasound (US)-responsive sustained CO release. Owing to the stabilization of $\text{Fe}_3\text{CO}_{12}$ within the silica framework, $\text{Fe}_3\text{CO}_{12}$ -MSNs not only decreased unwanted CO leakage during transport but also enabled US-responsive matrix degradation accompanied by sustained CO release at tumor sites, which prolongs the therapeutic window of CO and maximizes the synergy of SDT and CO therapy.

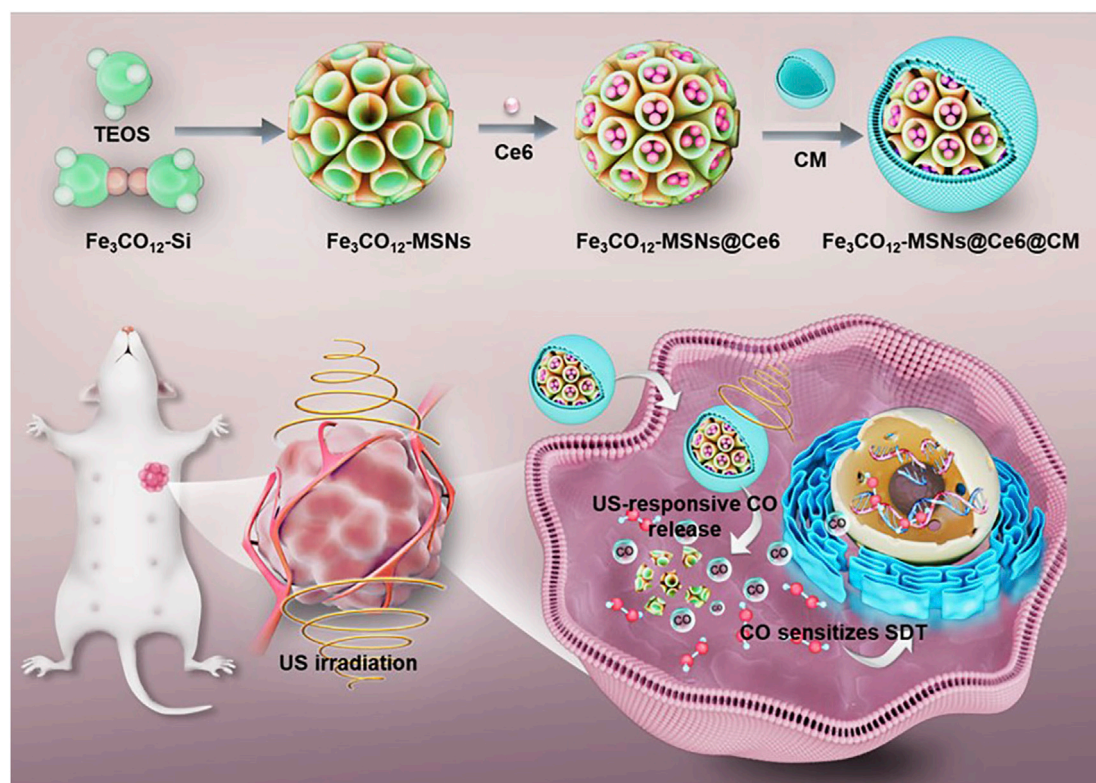
Results and Discussion: This nanoplatform-mediated combination therapies showed highly efficient antitumor effects and triggered a robust tumor-specific immune responses. When in combination with immune checkpoint blockers, the nanoplatform notably eradicate the breast cancer with low systematic toxicity. Overall, our work provides a promising nanoplatform with US-responsive and sustainable CO release for highly efficient and safe SDT/CO combined therapies.

KEYWORDS

sonodynamic therapy, gaseous therapy, breast cancer, hybrid materials, controlled release

1 Introduction

Breast cancer has become one of the most common malignancies that severely threatens women's health worldwide (Sun et al., 2017; Britt et al., 2020; Zhang et al., 2021). Traditional therapies, including surgery, radiotherapy, and chemotherapy, remain unsatisfactory because of their ineffectiveness and severe side effects (Castaneda and Strasser, 2017;



SCHEME 1 Schematic illustration of the fabrication of $\text{Fe}_3\text{CO}_{12}\text{-MSNs@Ce6@CM}$ and its application for SDT/CO combination therapies of breast cancer.

Keilty et al., 2020; Zuo et al., 2024). Photodynamic therapy (PDT) and sonodynamic therapy (SDT), which use laser and ultrasound (US) to activate photosensitizers and sonosensitizers for the production of reactive oxygen species (ROS), have gained considerable attention owing to their facile, controllable, and noninvasive characteristics (Sun et al., 2023; Zhang et al., 2023). Compared to PDT, SDT has performed well in more types of cancer because of its higher therapeutic depth (Zhao et al., 2024). Although more and more evidence has proven the effectiveness of SDT, SDT is still unable to eliminate cancer cells. In addition to SDT, gaseous therapy, such as oxygen (O_2), hydrogen (H_2), carbon monoxide (CO), and nitric oxide (NO), has been developed as a supporting remedy for cancer treatments (Yu et al., 2018; Chen et al., 2019). Among gaseous molecules, CO, as a critical gas transmitter that targets mitochondria and increases mitochondrial respiration, can sensitize tumor cells to ROS while protecting normal cells from oxidative stresses, thus considering a promising avenue to synergize with SDT (Zhao et al., 2019; Du et al., 2023). Unfortunately, direct inhalation of CO makes it difficult for CO to achieve the desired levels at tumor sites (Wang et al., 2019; Jin et al., 2021). Therefore, it is an urgent task to develop strategies for the efficient and controllable delivery of CO and sonosensitizers to maximize synergistic effects and minimize toxicity.

Metal carbonyl complexes (MCCs) are known as the most widely used CO-releasing molecules, which can reduce the side effects of direct inhalation (Wang et al., 2020; Zhang et al., 2024). Intensive efforts have been made to design various nanocarriers for preloading unstable MCCs to increase their accumulation at tumor

sites. However, it remains challenging to prevent premature CO leakage during the transport of nanodrugs and achieve synchronous production of ROS and CO during the combination of SDT and gaseous therapy. Compared with traditional organic and inorganic materials, organic-inorganic hybrid materials are more promising as delivery vehicles by virtue of their integration of the stability of inorganic materials and controllability and biodegradability inherited from organic materials (Erigoni and Diaz, 2021; Liu et al., 2021; Wang et al., 2024). Among them, MCC-bridged mesoporous silica nanoparticles (MSNs), which lock unstable MCCs in a stable mesoporous silica framework, have performed well in decreasing unwanted MCC leakage and achieving ROS-responsive release (Lu et al., 2023). However, the potential of MCC-bridged MSNs in SDT has not yet been fully explored.

In this study, we have fabricated an iron carbonyl ($\text{Fe}_3\text{CO}_{12}$)-bridged MSN ($\text{Fe}_3\text{CO}_{12}\text{-MSN}$) to preload sonosensitizers chlorine e6 (Ce6) for integrating SDT and CO gaseous therapy and then coated the cancer cell membrane to further improve the tumor target property. The prepared nanodrugs ($\text{Fe}_3\text{CO}_{12}\text{-MSNs@Ce6@CM}$) not only showed good stability in reducing CO leakage but also achieved biodegradation of the silica matrix and controllable release of CO in response to US irradiation. The sustainable release of CO triggered the maximal DNA damage to sensitize tumor cells to SDT and induce robust immunogenic cell death. Combined with immune checkpoint blockade therapy, the nanodrug enables the elimination of deeply metastatic tumors with low systemic toxicity. Our study provides a plausible strategy to integrate SDT and CO gaseous therapy for highly efficient and safe cancer treatments (Scheme 1).

2 Materials and methods

2.1 Preparation of Fe₃CO₁₂-MSNs

First, 0.25 g of Fe₃(CO)₁₂ was mixed with 0.353 g of 3-mercaptopropyltriethoxysilane (MPTES) in 50 mL of tetrahydrofuran (THF) and reacted at 70°C under nitrogen protection. After 2 h, the Fe₃CO₁₂-bridged organosilane (Fe₃CO₁₂-Si) was obtained by centrifugation and stored at –20°C for subsequent use. To synthesize Fe₃CO₁₂-MSNs, 0.1 g of triethanolamine (TEAH3) and 0.3 g of CTAB were added to 20 mL of deionized water and heated at 80°C for 30 min. Then, 0.2 g tetraethyl orthosilicate (TEOS) and Fe₃CO₁₂-bridged organosilane were added into the mixture as silica precursors and reacted for another 4 h. Finally, Fe₃CO₁₂-MSNs were obtained by centrifugation and stored at 4°C for subsequent experiments.

2.2 Cell membrane coating

4T1 cells were resuspended in 20 mL of hypotonic lysis buffer and subjected to sequential centrifugation. The obtained cell ghosts were then resuspended in 2 mL of water and sonicated for 10 min. To obtain cell membrane vesicles, the resulting ghosts were serially extruded through polycarbonate membranes. To coat the cell membranes onto Fe₃CO₁₂-MSNs@Ce6, Fe₃CO₁₂-MSNs@Ce6 was mixed with cell membrane vesicles in deionized water and extruded through 200-nm polycarbonate membranes. The prepared Fe₃CO₁₂-MSNs@Ce6@CM was lyophilized and stored at 4°C for subsequent experiments.

2.3 Biodegradation and CO release

To investigate the degradation of Fe₃CO₁₂-MSNs@Ce6@CM, Fe₃CO₁₂-MSNs@Ce6@CM and MSNs@Fe₃CO₁₂/Ce6@CM were dispersed in PBS solution with 0 or 100 μM of H₂O₂ under mild stirring. After 6 h, the X-ray US groups were exposed to US (40 kHz, 3.0 W/cm², 50% duty cycle) for 5 min. Then, the samples were collected on days 0, 1, and 3 for transmission electron microscopy (TEM, JEOL, Ltd., Japan), and the concentration of Si in the supernatant was measured using ICP-OES at predetermined time points.

We used the hemoglobin (Hb) assay to measure the CO release of Fe₃CO₁₂-MSNs@Ce6@CM in response to H₂O₂ and US irradiation. In brief, 20 μM of Hb was dissolved in the PBS solution with 0 or 100 μM of H₂O₂ under nitrogen protection in the presence of sodium dithionite. Then, Fe₃CO₁₂-MSNs@Ce6@CM and MSNs@Fe₃CO₁₂/Ce6@CM were added to the mixture solution. The mixture solution was irradiated by US for 5 min at 6 h. Next, the samples were collected at predetermined time points, and the absorbances of the samples were measured at 410 and 430 nm. The CO release was calculated using the following equation: concentration of CO = (I_{410nm} × 528.6 – I_{430 nm} × 304)/(I_{410nm} × 216.5 – I_{430 nm} × 442.4), where I_{430nm} and I_{410nm} represent the absorbance of the sample at wavelengths of 430 and 410 nm, respectively.

2.4 Cellular uptake and cytotoxicity

To assess the cellular uptake of Fe₃CO₁₂-MSNs@Ce6@CM, FITC-labeled Fe₃CO₁₂-MSNs@Ce6, MSNs@Fe₃CO₁₂/Ce6@CM, and Fe₃CO₁₂-MSNs@Ce6@CM were incubated with 4T1 cells for 4 h, respectively. Subsequently, the cells were fixed with paraformaldehyde for 10 min, stained with DAPI for 10 min, and observed using the confocal laser scanning microscope (CLSM; Olympus FV1000; Olympus, Tokyo, Japan). To quantify the cellular uptake, the cells were resuspended and detected using flow cytometry (BD Biosciences, Franklin Lakes, NJ, United States).

To investigate the cytotoxicity, 4T1 cells were planted onto 96-well plates at a density of 4 × 10³ cells/wells. After incubation overnight, Fe₃CO₁₂-MSNs@CM, Fe₃CO₁₂-MSNs@Ce6@CM, and MSNs@Fe₃CO₁₂/Ce6@CM were added into each well at various concentrations and incubated for 24 h. For the US treatment groups, 4T1 cells were exposed to US (40 kHz, 3.0 W/cm², 50% duty cycle) for 5 min at 6 h post-administration. Then, cell viability was analyzed using CCK-8 assays.

2.5 Biodistribution

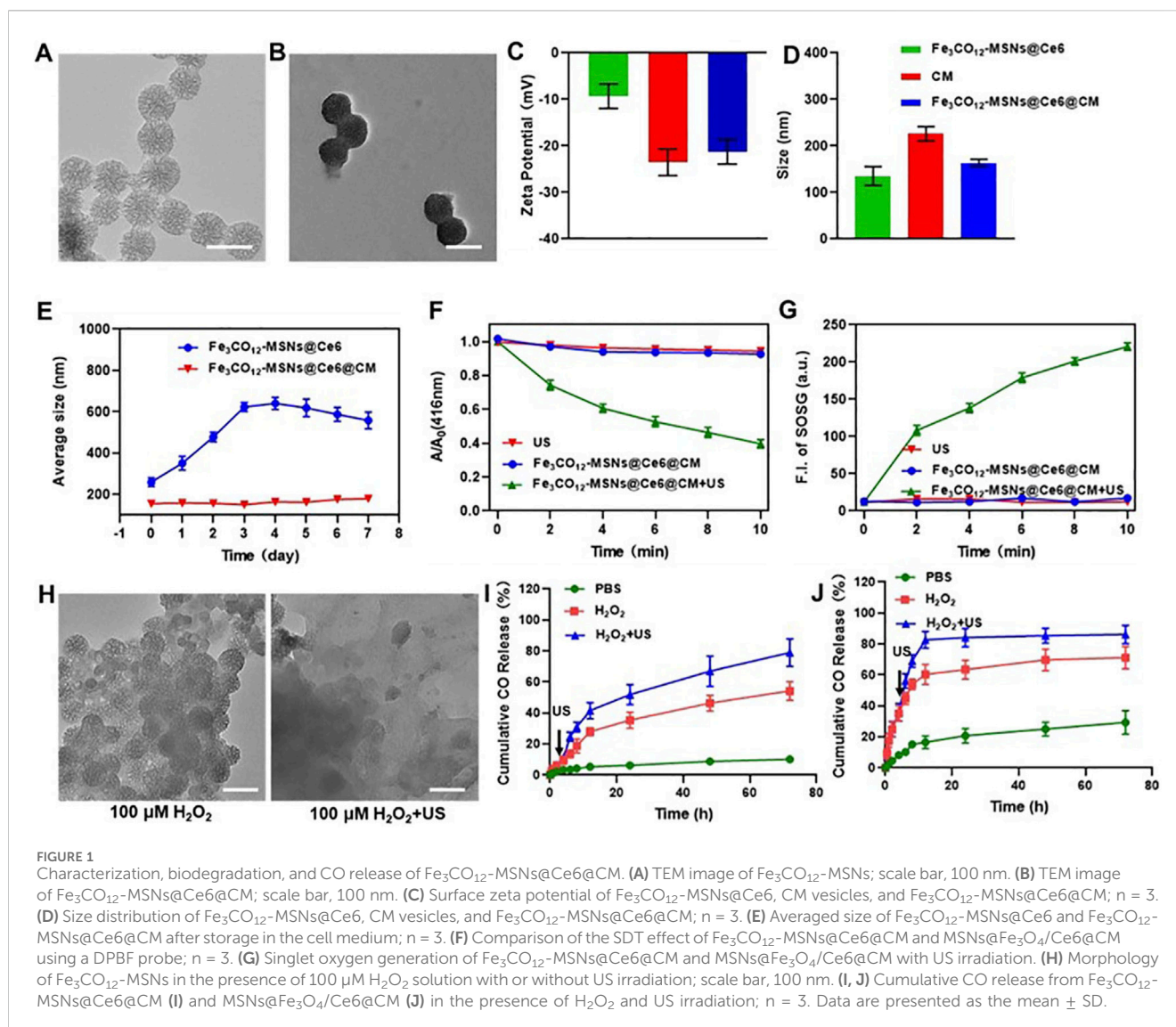
Animal experiments were approved by the Ethics Committee for the Use of Experimental Animals of Harbin Medical University and in accordance with the National Institute of Health Guide for the Care and Use of Laboratory Animals. To establish 4T1 tumor murine models, 1 mL of 4T1 cell suspension (5 × 10⁶) was injected into the mammary fat pads of female Balb/c mice. When the tumor volume reached approximately 800 mm³, 4T1 tumor-bearing mice were intravenously injected with Cy5.5-labeled Fe₃CO₁₂-MSNs@Ce6 and Fe₃CO₁₂-MSNs@Ce6@CM at a dose of 10 mg/kg. Then, major organs and tumors were harvested and weighed at different time points after administration and subsequently homogenized to measure fluorescence intensity.

2.6 Therapeutic effect *in vivo*

All the tumor models were randomized into seven groups and then intravenously injected with saline, Fe₃CO₁₂-MSNs@Ce6@CM (10 mg/kg), Fe₃CO₁₂-MSNs@Ce6@CM (10 mg/kg) plus αPD-L1 (1 mg/kg), and MSNs@Fe₃CO₁₂/Ce6@CM (10 mg/kg) plus αPD-L1 (1 mg/kg) in the absence or presence of US. Fe₃CO₁₂-MSNs@Ce6@CM or MSNs@Fe₃CO₁₂/Ce6@CM were administered every 3 days, and the tumor sites were irradiated with 1 MHz US at 1 W/cm² for 1 min at 8 h post-injection. For the αPD-L1 treatment groups, αPD-L1 was intravenously injected on day 6. Tumor volumes were measured every 3 days using a digital caliper and calculated using the formula: tumor volume = length × width² × 0.52. All the mice were euthanized on day 23, and the tumors were harvested and weighed.

2.7 Systemic toxicity evaluation

4T1 tumor-bearing mice were intravenously injected with Fe₃CO₁₂-MSNs@Ce6@CM (10 mg/kg) and Fe₃CO₁₂-MSNs@



Ce6@CM (10 mg/kg) plus $\alpha\text{PD-L1}$ (1 mg/kg) and exposed to 1 Hz US at 1 W/cm^2 for 1 min. All the mice were euthanized on day 21. The major organs, including the liver, spleen, kidneys, heart, and lungs, were harvested, fixed, and stained with hematoxylin–eosin (H&E). Blood was collected, and the levels of aspartate aminotransferase (AST), alanine aminotransferase (ALT), alkaline phosphatase (ALP), and blood urea nitrogen (BUN) were detected using ELISA kits.

2.8 Statistics

GraphPad Prism was used for statistical analysis, with Student's t-test applied for comparing two groups, while one-way ANOVA (Tukey's multiple comparison test) or two-way ANOVA (Tukey's and Sidak's multiple comparisons test) was used for analyzing differences among multiple groups. Data are presented as the mean \pm SD, with significance levels denoted as * $P < 0.05$, ** $P < 0.01$, and *** $P < 0.001$, where $P < 0.05$ indicates statistical significance.

3 Results and discussion

We prepared $\text{Fe}_3\text{CO}_{12}\text{-MSNs}$ using a sol–gel method, with tetraethyl orthosilicate (TEOS) and $\text{Fe}_3\text{CO}_{12}$ -bridged organosilane as the precursors and cetyltrimethylammonium bromide (CTAB) as a structure-directing agent. As shown in Figure 1A, $\text{Fe}_3\text{CO}_{12}\text{-MSNs}$ exhibited a spherical shape with a diameter of $\sim 100 \text{ nm}$. N_2 adsorption–desorption isotherms indicated that $\text{Fe}_3\text{CO}_{12}\text{-MSNs}$ had a pore volume of $1.02 \text{ cm}^3/\text{g}$, a larger surface area of $613.5 \text{ m}^2/\text{g}$, and uniform pore size distribution of 3.6 nm , which suggested the excellent drug-loading capability of $\text{Fe}_3\text{CO}_{12}\text{-MSNs}$ (Supplementary Figure S1). The drug-loading content of $\text{Fe}_3\text{CO}_{12}\text{-MSNs@Ce6}$ was calculated to be 9.7%. To improve the colloidal stability and tumor targeting, we coated murine breast cancer 4T1 cell membranes onto the surface of $\text{Fe}_3\text{CO}_{12}\text{-MSNs}$. The formed $\text{Fe}_3\text{CO}_{12}\text{-MSNs@Ce6@CM}$ showed an obvious core-shell structure with a thin lipid shell and a slightly larger hydrodynamic size than that of $\text{Fe}_3\text{CO}_{12}\text{-MSNs@Ce6}$ (Figures 1B,C). Furthermore, the surface potential of $\text{Fe}_3\text{CO}_{12}\text{-MSNs@Ce6@CM}$ was more negative than $\text{Fe}_3\text{CO}_{12}\text{-MSNs@Ce6}$, which was approximate to that of cell membranes (Figure 1D). These results confirmed the successful coating of cell membranes onto

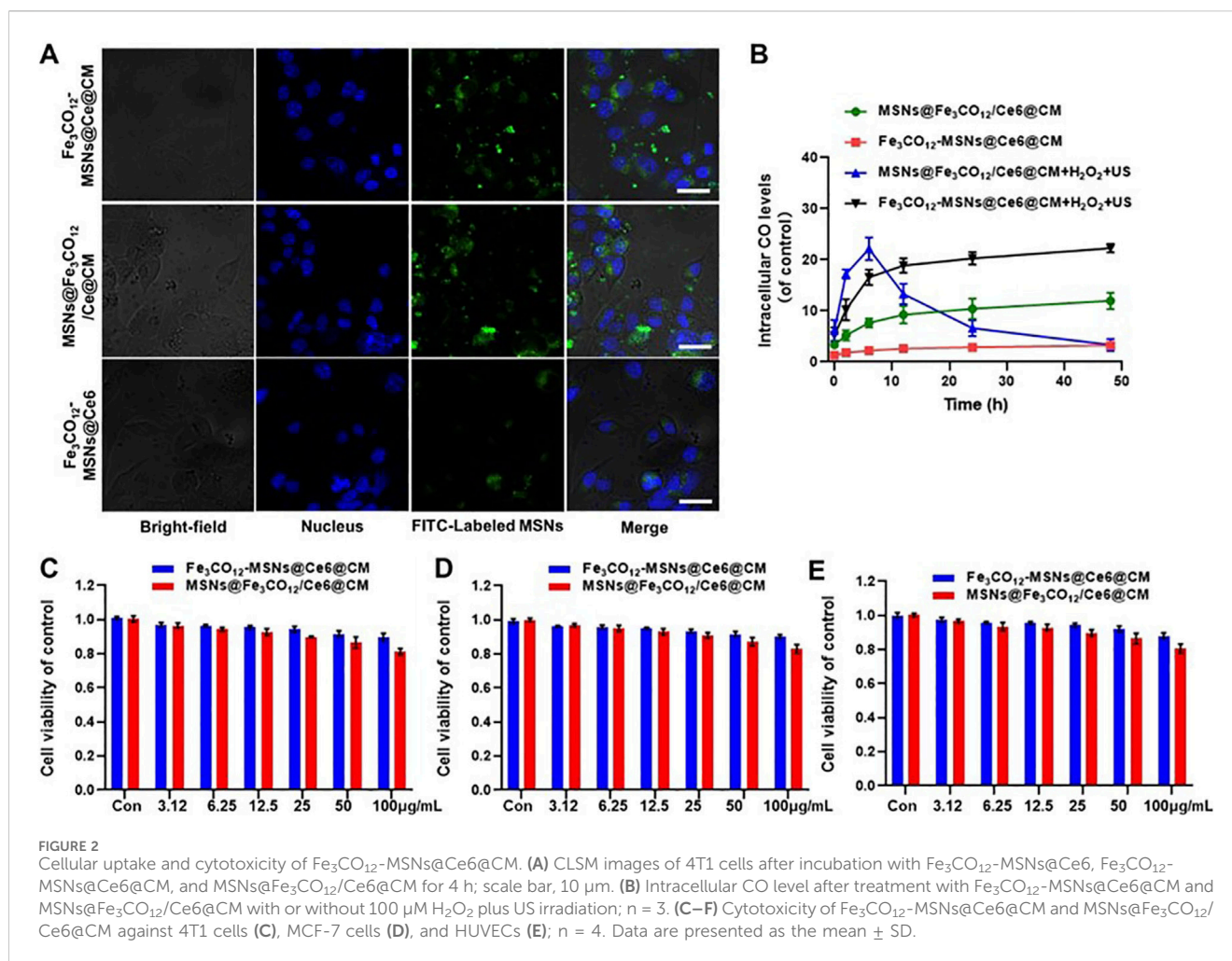
$\text{Fe}_3\text{CO}_{12}\text{-MSNs@Ce6}$. Additionally, $\text{Fe}_3\text{CO}_{12}\text{-MSNs@Ce6@CM}$ displayed good monodispersity after storage in cell medium for 24 h, whereas aggregation appeared in $\text{Fe}_3\text{CO}_{12}\text{-MSNs@Ce6}$ in the cell medium, indicating that the coating of cell membranes improved the colloidal stability of $\text{Fe}_3\text{CO}_{12}\text{-MSNs@Ce6}$ (Figure 1E). To explore the potential of $\text{Fe}_3\text{CO}_{12}\text{-MSNs@Ce6@CM}$ as sonosensitizers, we detected the ROS generation of $\text{Fe}_3\text{CO}_{12}\text{-MSNs@Ce6@CM}$ under irradiation using a 1,3-diphenylisobenzofuran (DPBF) probe. As shown in Figure 1F, $\text{Fe}_3\text{CO}_{12}\text{-MSNs@Ce6@CM}$ did not produce ROS in the absence of US. However, the generation of ROS was detected when $\text{Fe}_3\text{CO}_{12}\text{-MSNs@Ce6@CM}$ was irradiated by US. Moreover, the amount of ROS was increased with the extension of US irradiation. Consistent results regarding the generation of singlet oxygen ($^1\text{O}_2$) were measured using a singlet oxygen sensor green (SOSG) probe. These results indicated the potential of $\text{Fe}_3\text{CO}_{12}\text{-MSNs@Ce6}$ to function as effective sonosensitizers for cancer SDT.

We next investigated the degradation and release behavior of $\text{Fe}_3\text{CO}_{12}\text{-MSNs@Ce6@CM}$ in response to US irradiation. $\text{Fe}_3\text{CO}_{12}\text{-MSNs}$ collapsed into irregular aggregates in the PBS solution containing 100 μM H_2O_2 , simulating a tumor microenvironment, but were unable to further disassemble (Figure 1G). In contrast, $\text{Fe}_3\text{CO}_{12}\text{-MSNs}$ completely degrade in 100 μM H_2O_2 with US irradiation. This phenomenon could be explained by the cleavage of the Fe–CO bond by the strong oxidative H_2O_2 , while the generation of ROS by US inside the MSNs directly breaks the Fe–CO bond to promote degradation. The ROS- and US-dual-responsive degradation property might contribute to improving the specificity of CO delivery in tumors. We subsequently explored the CO release from $\text{Fe}_3\text{CO}_{12}\text{-MSNs@Ce6@CM}$ in PBS or 100 μM H_2O_2 with or without US. To further verify the advantages of $\text{Fe}_3\text{CO}_{12}\text{-MSNs@Ce6@CM}$ in CO release, inorganic MSNs were prepared to load Ce6 and $\text{Fe}_3\text{CO}_{12}$ and coated with 4T1 cell membranes ($\text{MSNs@Fe}_3\text{CO}_{12}/\text{Ce6@CM}$) as a comparison. The increased hydrodynamic size and negative surface potential of $\text{MSNs@Fe}_3\text{CO}_{12}/\text{Ce6@CM}$ indicated the successful coating of CM onto $\text{MSNs@Fe}_3\text{CO}_{12}/\text{Ce6}$ (Supplementary Figure S2). Additionally, the coating of CM improved the colloidal stability of $\text{MSNs@Fe}_3\text{CO}_{12}/\text{Ce6@CM}$ (Supplementary Figure S3). Notably, MSNs showed a similar morphology to $\text{Fe}_3\text{CO}_{12}\text{-MSN}$ but could not degrade in 100 μM H_2O_2 solution or under US irradiation (Supplementary Figure S4). Furthermore, both $\text{Fe}_3\text{CO}_{12}\text{-MSNs@Ce6@CM}$ and $\text{MSNs@Fe}_3\text{CO}_{12}/\text{Ce6@CM}$ showed ROS- and US-dual-responsive CO release behavior. However, CO release from $\text{Fe}_3\text{CO}_{12}\text{-MSNs@Ce6@CM}$ was more sustained in the presence of H_2O_2 and H_2O_2 plus US than that from $\text{MSNs@Fe}_3\text{CO}_{12}/\text{Ce6@CM}$ under the same stimulus. The sustainable CO release behavior may help maintain the therapeutic concentration of CO in tumors for prolonging its therapeutic window since CO has high diffusivity and poor solubility, which may address the challenge of therapeutic gases failing to achieve prolonged high-concentration enrichment at target sites. On the other hand, the leakage of CO from $\text{MSNs@Fe}_3\text{CO}_{12}/\text{Ce6@CM}$ in the PBS solution reached 29.3% without 100 μM H_2O_2 or US irradiation, whereas only 10.1% CO was released from $\text{Fe}_3\text{CO}_{12}\text{-MSNs@Ce6@CM}$ after 24 h. These results suggested that $\text{Fe}_3\text{CO}_{12}\text{-MSNs@Ce6@CM}$ were much more stable than $\text{MSNs@Fe}_3\text{CO}_{12}/\text{Ce6@CM}$, which helped decrease unwanted CO leakage during circulation.

Encouraged by the US-activated ROS generation and US-controllable CO release, we sought to investigate the cytotoxicity of $\text{Fe}_3\text{CO}_{12}\text{-MSNs@Ce6@CM}$ *in vitro*. Endocytosis plays a vital role

in cytotoxicity. Therefore, we first investigated the cellular uptake of $\text{Fe}_3\text{CO}_{12}\text{-MSNs@Ce6}$, $\text{Fe}_3\text{CO}_{12}\text{-MSNs@Ce6@CM}$, and $\text{MSNs@Fe}_3\text{CO}_{12}/\text{Ce6@CM}$ in 4T1 cells. All the nanoparticles could be taken up by 4T1 cells, and $\text{Fe}_3\text{CO}_{12}\text{-MSNs@Ce6@CM}$ exhibited a similar cellular uptake to $\text{MSNs@Fe}_3\text{CO}_{12}/\text{Ce6@CM}$ (Figure 2A; Supplementary Figure S5). Additionally, $\text{Fe}_3\text{CO}_{12}\text{-MSNs@Ce6@CM}$ showed higher cellular internalization efficiency than $\text{MSNs@Fe}_3\text{CO}_{12}/\text{Ce6}$, which was attributed to the coating of cancer cell membranes. Then, we investigated the intracellular CO delivery using the FL-CO-1 probe, which could generate 480 nm fluorescence after binding with CO. As shown in Figure 2B, lower fluorescent intensity was detected in $\text{Fe}_3\text{CO}_{12}\text{-MSNs@Ce6@CM}$ than in $\text{MSNs@Fe}_3\text{CO}_{12}/\text{Ce6@CM}$ without the stimulus of H_2O_2 or US, indicating that $\text{Fe}_3\text{CO}_{12}\text{-MSNs@Ce6@CM}$ had better stability than $\text{MSNs@Fe}_3\text{CO}_{12}/\text{Ce6@CM}$. Notably, intracellular CO from $\text{Fe}_3\text{CO}_{12}\text{-MSNs@Ce6@CM}$ showed a more sustained presence than that from $\text{MSNs@Fe}_3\text{CO}_{12}/\text{Ce6@CM}$ in the presence of H_2O_2 and US, owing to the sustainable CO release of $\text{Fe}_3\text{CO}_{12}\text{-MSNs@Ce6@CM}$, which might contribute to enhancing the efficacy of CO therapy in tumors when US irradiation is applied. Then, we measured the cytotoxicity of $\text{Fe}_3\text{CO}_{12}\text{-MSNs@Ce6@CM}$ toward 4T1 cells, MCF-7 cells, and HUVECs after 24 h using CCK-8 assays. As shown in Figures 2C–E and Supplementary Figure S6, $\text{MSNs@Fe}_3\text{CO}_{12}/\text{Ce6@CM}$ showed slightly higher cytotoxicity than $\text{Fe}_3\text{CO}_{12}\text{-MSNs@Ce6@CM}$ without US irradiation after 24 h and 72 h of incubation, likely due to the easier leakage of CO. The lower cytotoxicity of $\text{Fe}_3\text{CO}_{12}\text{-MSNs@Ce6@CM}$ suggested that it had better biomedical application prospects.

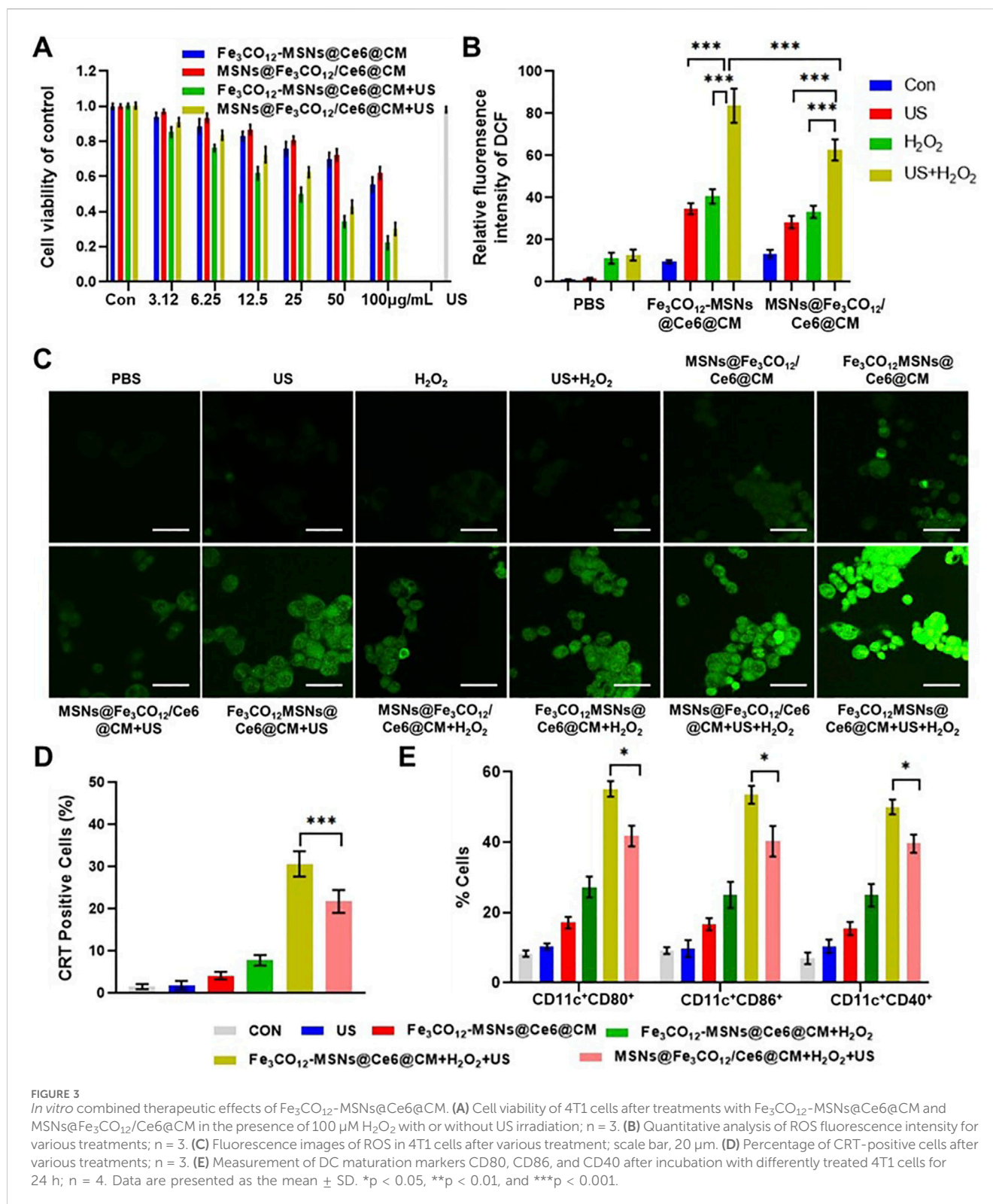
To further explore the therapeutic effect of $\text{Fe}_3\text{CO}_{12}\text{-MSNs@Ce6@CM}$ *in vitro*, 4T1 cells were incubated with various concentrations of $\text{Fe}_3\text{CO}_{12}\text{-MSNs@Ce6@CM}$, $\text{Fe}_3\text{CO}_{12}\text{-MSNs@Ce6@CM}$, and $\text{MSNs@Fe}_3\text{CO}_{12}/\text{Ce6@CM}$ with the addition of 100 μM , simulating a tumor microenvironment in the absence or presence of US irradiation. As shown in Figure 3A, both $\text{Fe}_3\text{CO}_{12}\text{-MSNs@Ce6@CM}$ and $\text{MSNs@Fe}_3\text{CO}_{12}/\text{Ce6@CM}$ showed concentration-dependent toxicity toward 4T1 cells. When exposed to US irradiation, the therapeutic effects of $\text{Fe}_3\text{CO}_{12}\text{-MSNs@Ce6@CM}$ and $\text{MSNs@Fe}_3\text{CO}_{12}/\text{Ce6@CM}$ were obviously enhanced, indicating their CO and SDT combination therapies. Notably, $\text{Fe}_3\text{CO}_{12}\text{-MSNs@Ce6@CM}$ induced more 4T1 cell death than $\text{MSNs@Fe}_3\text{CO}_{12}/\text{Ce6@CM}$ in the presence of 100 μM H_2O_2 and US irradiation, owing to the sustained CO release of $\text{Fe}_3\text{CO}_{12}\text{-MSNs@Ce6@CM}$. For further validation, we measured the intracellular ROS level after various treatments using 2',7'-dichlorofluorescein diacetate (DCFH-DA), a nonfluorescent probe that can react with intracellular ROS to form fluorescent 2',7'-dichlorofluorescein (DCF). As shown in Figures 3B,C, more intracellular ROS was detected in the cells after the treatment with $\text{MSNs@Fe}_3\text{CO}_{12}/\text{Ce6@CM}$ than that with $\text{Fe}_3\text{CO}_{12}\text{-MSNs@Ce6@CM}$ in the absence of US and H_2O_2 , possibly due to the more leakage of CO from $\text{MSNs@Fe}_3\text{CO}_{12}/\text{Ce6@CM}$. Additionally, either US or H_2O_2 could increase intracellular ROS generation of $\text{MSNs@Fe}_3\text{CO}_{12}/\text{Ce6@CM}$ and $\text{Fe}_3\text{CO}_{12}\text{-MSNs@Ce6@CM}$, and the combination of US and H_2O_2 induced more ROS generation of $\text{MSNs@Fe}_3\text{CO}_{12}/\text{Ce6@CM}$ and $\text{Fe}_3\text{CO}_{12}\text{-MSNs@Ce6@CM}$. Furthermore, $\text{Fe}_3\text{CO}_{12}\text{-MSNs@Ce6@CM}$ led to the highest ROS compared to $\text{MSNs@Fe}_3\text{CO}_{12}/\text{Ce6@CM}$ under H_2O_2 and US stimulation. These results indicated that $\text{Fe}_3\text{CO}_{12}\text{-MSNs@Ce6@CM}$



CM had great potential in sensitizing SDT, owing to its sustained CO release property. Considering that SDT could induce immunogenic cell death (ICD) to promote antitumor immune responses, we detected the ability of $\text{Fe}_3\text{CO}_{12}$ -MSNs@Ce6@CM to induce ICD effects by measuring calreticulin (CRT) exposure and the secretion of chromatin-binding protein high-mobility group B1 (HMGB1). As expected, $\text{Fe}_3\text{CO}_{12}$ -MSNs@Ce6@CM triggers more CRT-positive cells and higher release of HMGB1 than MSNs@ $\text{Fe}_3\text{CO}_{12}$ /Ce6@CM in the presence of US and H_2O_2 (Figure 3D; Supplementary Figure S7). To further evaluate the immunological effects of $\text{Fe}_3\text{CO}_{12}$ -MSNs@Ce6@CM-mediated combination therapies, we incubated 4T1 cells after various treatments with dendritic cells (DCs). We found that $\text{Fe}_3\text{CO}_{12}$ -MSNs@Ce6@CM plus US-treated 4T1 cells induced the most DC maturation (Figure 3E). These results indicated that $\text{Fe}_3\text{CO}_{12}$ -MSNs@Ce6@CM-mediated combination therapies could activate a strong antitumor immune response.

After demonstrating the anticancer effect and ICD induction of $\text{Fe}_3\text{CO}_{12}$ -MSNs@Ce6@CM *in vitro*, we explored its therapeutic effect *in vivo*. Owing to the coating of cancer cell membranes, $\text{Fe}_3\text{CO}_{12}$ -MSNs@Ce6@CM exhibited prolonged blood circulation and higher tumor accumulation efficiency than $\text{Fe}_3\text{CO}_{12}$ -MSNs@Ce6@CM (Figures 4A–C). The tumor accumulation of $\text{Fe}_3\text{CO}_{12}$ -MSNs@Ce6@CM peaked at 8 h of intravenous injection. Additionally, MSNs@ $\text{Fe}_3\text{CO}_{12}$ /Ce6@CM exhibited a similar tumor

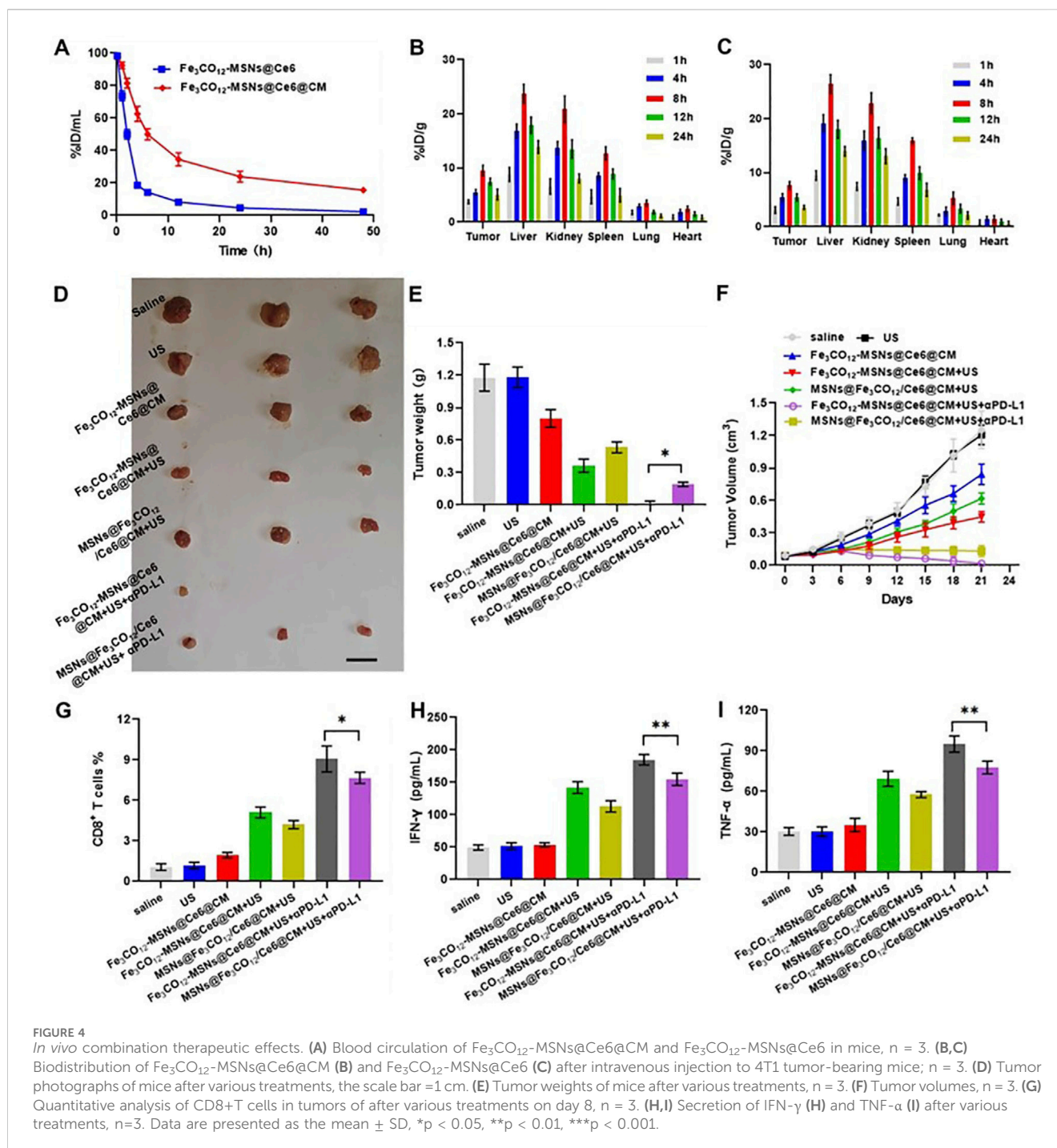
accumulation efficiency to $\text{Fe}_3\text{CO}_{12}$ -MSNs@Ce6@CM (Supplementary Figure S8). Thus, we used US to irradiate tumors 8 h after administration. Then, we evaluated the antitumor effect of $\text{Fe}_3\text{CO}_{12}$ -MSNs@Ce6@CM in the presence of US in combination with immune checkpoint blockers. As shown in Figures 4D–F, a single US had a negligible inhibitory effect on tumor progression. $\text{Fe}_3\text{CO}_{12}$ -MSNs@Ce6@CM slightly delayed the tumor growth, possibly due to the partial release of CO. Notably, $\text{Fe}_3\text{CO}_{12}$ -MSNs@Ce6@CM plus US showed a remarkable antitumor effect, which displayed higher tumor inhibition rates (69.2%) than MSNs@ $\text{Fe}_3\text{CO}_{12}$ /Ce6@CM plus US (54.4%), further confirming that $\text{Fe}_3\text{CO}_{12}$ -MSNs@Ce6@CM had excellent SDT sensitization effect owing to its sustained CO release properties. Furthermore, $\text{Fe}_3\text{CO}_{12}$ -MSNs@Ce6@CM plus US exhibited near-complete tumor eradication when combined with PD-1 antibodies ($\alpha\text{PD-1}$), showing superior efficacy to MSNs@ $\text{Fe}_3\text{CO}_{12}$ /Ce6@CM plus US with $\alpha\text{PD-1}$. Moreover, $\text{Fe}_3\text{CO}_{12}$ -MSNs@Ce6@CM plus US with $\alpha\text{PD-1}$ resulted in the most CD8⁺ T cells in tumors and the highest release of proinflammatory cytokines, including interleukin-6 (IL-6), interferon- γ (IFN- γ), and tumor necrosis factor- α (TNF- α) (Figures 4G–I; Supplementary Figure S9). These results indicated that $\text{Fe}_3\text{CO}_{12}$ -MSNs@Ce6@CM-mediated SDT boosted a strong immune activation and thus exerted a



synergistic antitumor effect with immune checkpoint blockade treatment to suppress tumor progression.

Biosafety is an important concern for the application of nanomedicines. Therefore, we investigated the systemic toxicity of $\text{Fe}_3\text{CO}_{12}$ -MSNs@Ce6@CM-mediated combination treatments by detecting the body weights and serum biochemistry indexes, along

with the histology of the major organs. Encouragingly, $\text{Fe}_3\text{CO}_{12}$ -MSNs@Ce6@CM plus US and $\text{Fe}_3\text{CO}_{12}$ -MSNs@Ce6@CM plus US with $\alpha\text{PD-1}$ did not lead to a significant decrease in the body weight of mice and obvious changes in serum biochemistry indexes compared with the control groups (Figures 5B–E; Supplementary Figure S10). Additionally, H&E staining indicated that no pathological change was

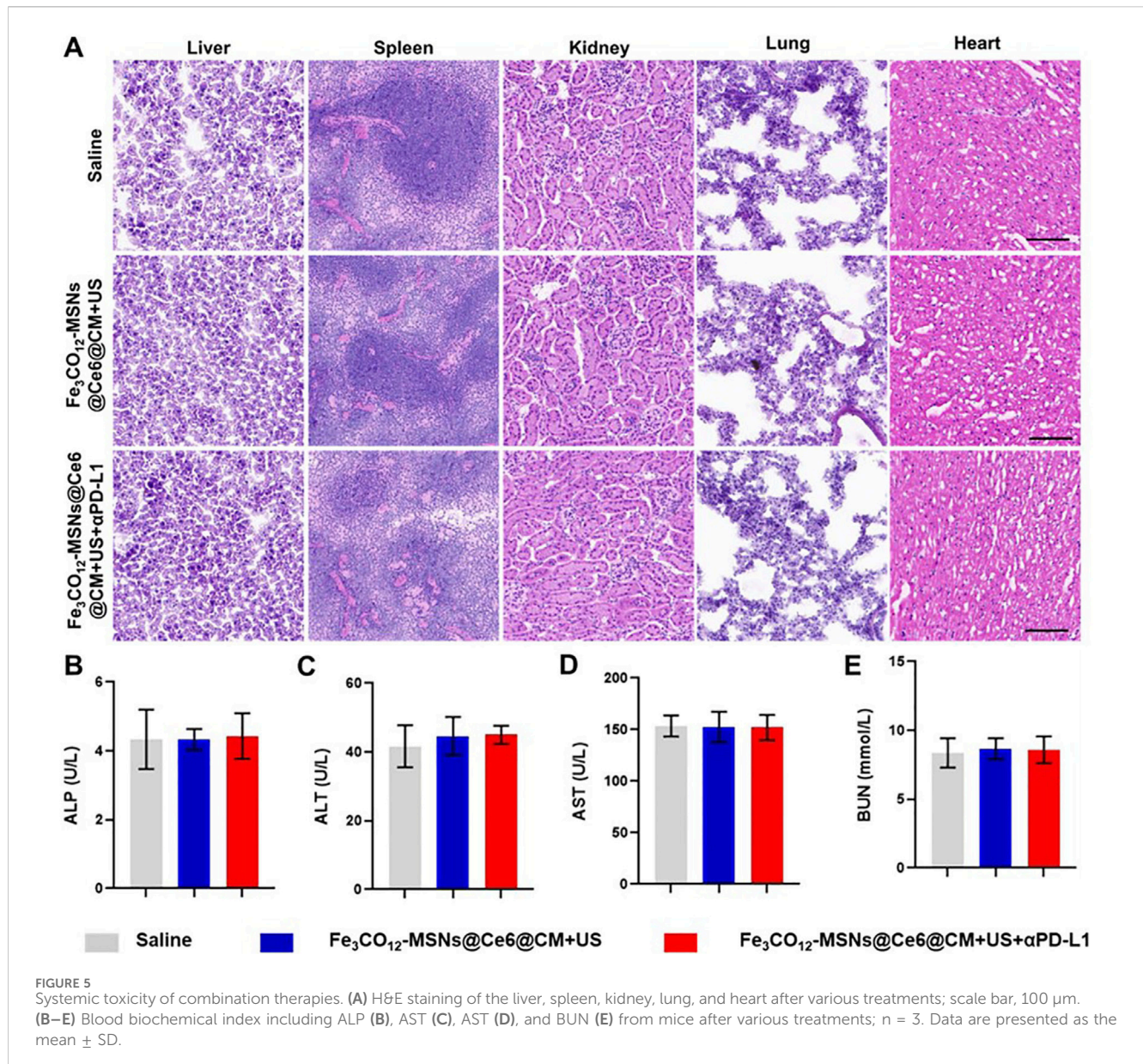


observed in major organs, including the liver, spleen, kidney, lung, and heart, of mice after the treatments with $\text{Fe}_3\text{CO}_{12}$ -MSNs@Ce6@CM plus US or $\text{Fe}_3\text{CO}_{12}$ -MSNs@Ce6@CM plus US with $\alpha\text{PD-1}$ (Figure 5A). These results confirmed that $\text{Fe}_3\text{CO}_{12}$ -MSNs@Ce6@CM-mediated combination therapies had low side effects.

4 Conclusion

In summary, we fabricated US-responsive $\text{Fe}_3\text{CO}_{12}$ -MSNs to load sonosensitizer Ce6 for enhanced SDT of breast cancer.

$\text{Fe}_3\text{CO}_{12}$ -MSNs showed high Ce6-loading ability, ultrastability, and sustained CO release with the stimulus of US irradiation and H_2O_2 addition, thus decreasing unwanted CO leakage under physiological conditions and prolonging the therapeutic window in tumors, which effectively sensitized SDT. After coating with cancer cell membranes, $\text{Fe}_3\text{CO}_{12}$ -MSNs@Ce6@CM exhibited increased blood circulation time and enhanced tumor-targeting ability. The *in vitro* and *in vivo* results indicated that $\text{Fe}_3\text{CO}_{12}$ -MSNs@Ce6@CM-mediated combination treatments of SDT and CO gaseous therapy possessed an excellent antitumor effect and



simultaneously elicited an outstanding ICD effect, which was better than that of traditional $\text{Fe}_3\text{CO}_{12}$ -loaded MSNs. When combined with $\alpha\text{PD-1}$, $\text{Fe}_3\text{CO}_{12}\text{-MSNs@Ce6@CM}$ plus US exerted almost complete elimination of primary 4T1 tumors and suppression of metastatic tumors with low systemic toxicity. Our work offers a promising CO-releasing nanoplatform with organic–inorganic bridged architectures for US-activated cancer combination therapies.

Data availability statement

The original contributions presented in the study are included in the article/Supplementary Material; further inquiries can be directed to the corresponding author.

Ethics statement

The animal study was approved by the Ethics Committee for the Use of Experimental Animals of Mudanjiang Medical University. The study was conducted in accordance with the local legislation and institutional requirements.

Author contributions

CF: writing – original draft, conceptualization, methodology, and investigation. SS: methodology, writing – original draft, software, validation, and data curation. XZ: formal analysis, writing – original draft, investigation, resources, and visualization. JW: resources, writing – original draft,

validation, and data curation. QM: formal analysis, investigation, and writing – original draft. TW: supervision, project administration, writing – review and editing, and conceptualization.

Funding

The author(s) declare that financial support was received for the research and/or publication of this article. This research was supported by the Science and Technology program of the Health Commission of Heilongjiang Province (grant number: 20240909020469), China.

Conflict of interest

The authors declare that the research was conducted in the absence of any commercial or financial relationships that could be construed as a potential conflict of interest.

References

- Britt, K. L., Cuzick, J., and Phillips, K.-A. (2020). Key steps for effective breast cancer prevention. *Nat. Rev. Cancer* 20, 417–436. doi:10.1038/s41568-020-0266-x
- Castaneda, S. A., and Strasser, J. (2017). Updates in the treatment of breast cancer with radiotherapy. *Surg. Oncol. Clin.* 26, 371–382. doi:10.1016/j.soc.2017.01.013
- Chen, L., Zhou, S.-F., Su, L., and Song, J. (2019). Gas-mediated cancer bioimaging and therapy. *ACS nano* 13, 10887–10917. doi:10.1021/acsnano.9b04954
- Du, Z., Wang, X., Zhang, X., Gu, Z., Fu, X., Gan, S., et al. (2023). X-ray-triggered carbon monoxide and manganese dioxide generation based on scintillating nanoparticles for cascade cancer radiosensitization. *Angew. Chem. Int. Ed.* 62, e202302525. doi:10.1002/anie.202302525
- Erigoni, A., and Diaz, U. (2021). Porous silica-based organic-inorganic hybrid catalysts: a review. *Catalysts* 11, 79. doi:10.3390/catal11010079
- Jin, Z., Duo, Y., Li, Y., Qiu, M., Jiang, M., Liu, Q., et al. (2021). A novel NIR-responsive CO gas-releasing and hyperthermia-generating nanomedicine provides a curative approach for cancer therapy. *Nano Today* 38, 101197. doi:10.1016/j.nantod.2021.101197
- Keilty, D., Namini, S. N., Swain, M., Maganti, M., Cil, T. D., Mccready, D. R., et al. (2020). Patterns of recurrence and predictors of survival in breast cancer patients treated with neoadjuvant chemotherapy, surgery, and radiation. *Int. J. Radiat. Oncology* Biology* Phys.* 108, 676–685. doi:10.1016/j.ijrobp.2020.04.044
- Liu, X., Wu, Y., Zhao, X., and Wang, Z. (2021). Fabrication and applications of bioactive chitosan-based organic-inorganic hybrid materials: a review. *Carbohydr. Polym.* 267, 118179. doi:10.1016/j.carbpol.2021.118179
- Lu, J., Chen, F., Xie, X., Wu, Z., Chen, Y., Zhang, Y., et al. (2023). X-ray-controllable release of carbon monoxide potentiates radiotherapy by ultrastable hybrid nanoreservoirs. *Biomaterials* 302, 122313. doi:10.1016/j.biomaterials.2023.122313
- Sun, L., Cao, Y., Li, W., Wang, L., Ding, P., Lu, Z., et al. (2023). Perovskite-type manganese vanadate sonosensitizers with biodegradability for enhanced sonodynamic therapy of cancer. *Small* 19, 2300101. doi:10.1002/smll.202300101
- Sun, Y.-S., Zhao, Z., Yang, Z.-N., Xu, F., Lu, H.-J., Zhu, Z.-Y., et al. (2017). Risk factors and preventions of breast cancer. *Int. J. Biol. Sci.* 13, 1387–1397. doi:10.7150/ijbs.21635

Generative AI statement

The author(s) declare that no Generative AI was used in the creation of this manuscript.

Publisher's note

All claims expressed in this article are solely those of the authors and do not necessarily represent those of their affiliated organizations, or those of the publisher, the editors and the reviewers. Any product that may be evaluated in this article, or claim that may be made by its manufacturer, is not guaranteed or endorsed by the publisher.

Supplementary material

The Supplementary Material for this article can be found online at: <https://www.frontiersin.org/articles/10.3389/fbioe.2025.1615481/full#supplementary-material>

- Wang, S.-B., Zhang, C., Chen, Z.-X., Ye, J.-J., Peng, S.-Y., Rong, L., et al. (2019). A versatile carbon monoxide nanogenerator for enhanced tumor therapy and anti-inflammation. *ACS nano* 13, 5523–5532. doi:10.1021/acsnano.9b00345
- Wang, X.-S., Zeng, J.-Y., Li, M.-J., Li, Q.-R., Gao, F., and Zhang, X.-Z. (2020). Highly stable iron carbonyl complex delivery nanosystem for improving cancer therapy. *ACS nano* 14, 9848–9860. doi:10.1021/acsnano.0c02516
- Wang, Z., Chen, F., Cao, Y., Zhang, F., Sun, L., Yang, C., et al. (2024). An engineered nanoplatform with tropism toward irradiated glioblastoma augments its radioimmunotherapy efficacy. *Adv. Mater.* 36, 2314197. doi:10.1002/adma.202314197
- Yu, L., Hu, P., and Chen, Y. (2018). Gas-generating nanoplatforms: material chemistry, multifunctionality, and gas therapy. *Adv. Mater.* 30, 1801964. doi:10.1002/adma.201801964
- Zhang, B., Lin, L., Mao, J., Mo, W., Li, Z., Wang, S., et al. (2023). Self-oxygenated co-assembled biomimetic nanoplatform for enhanced photodynamic therapy in hypoxic tumor. *Chin. Chem. Lett.* 34, 108518. doi:10.1016/j.ccllet.2023.108518
- Zhang, C., Huang, S., Ding, K., Wu, H., Li, M., Li, T., et al. (2024). Tumor-targeted CO nanodelivery system design and therapy for hepatocellular carcinoma. *Mol. Pharm.* 21, 5015–5027. doi:10.1021/acs.molpharmaceut.4c00437
- Zhang, Y.-N., Xia, K.-R., Li, C.-Y., Wei, B.-L., and Zhang, B. (2021). Review of breast cancer pathological image processing. *BioMed Res. Int.* 2021, 1994764. doi:10.1155/2021/1994764
- Zhao, B., Zhao, P., Jin, Z., Fan, M., Meng, J., and He, Q. (2019). Programmed ROS/CO-releasing nanomedicine for synergetic chemodynamic-gas therapy of cancer. *J. Nanobiotechnology* 17, 75–12. doi:10.1186/s12951-019-0507-x
- Zhao, Q., Zhao, Y., Zhong, S., Yue, Z., Jiang, Z., Wang, S., et al. (2024). Urchin-like piezoelectric ZnSnO₃/Cu₃P pn heterojunction for enhanced cancer sonodynamic therapy. *Chin. Chem. Lett.* 35, 109644. doi:10.1016/j.ccllet.2024.109644
- Zuo, S., Wang, Z., Jiang, X., Zhao, Y., Wen, P., Wang, J., et al. (2024). Regulating tumor innervation by nanodrugs potentiates cancer immunotherapy and relieve chemotherapy-induced neuropathic pain. *Biomaterials* 309, 122603. doi:10.1016/j.biomaterials.2024.122603